

Efficient three-color white organic light-emitting diodes with a spaced multilayer emitting structure

Fei Yan, Guichuan Xing, Rui Chen, Hilmi Volkan Demir, Handong Sun, Tze Chien Sum, and Xiao Wei Sun

Citation: [Applied Physics Letters](#) **106**, 023302 (2015); doi: 10.1063/1.4905599

View online: <http://dx.doi.org/10.1063/1.4905599>

View Table of Contents: <http://scitation.aip.org/content/aip/journal/apl/106/2?ver=pdfcov>

Published by the [AIP Publishing](#)

Articles you may be interested in

[Using interlayer step-wise triplet transfer to achieve an efficient white organic light-emitting diode with high color-stability](#)

Appl. Phys. Lett. **104**, 193303 (2014); 10.1063/1.4876215

[Full phosphorescent white-light organic light-emitting diodes with improved color stability and efficiency by fine tuning primary emission contributions](#)

AIP Advances **4**, 027103 (2014); 10.1063/1.4865209

[Organic light-emitting diodes for lighting: High color quality by controlling energy transfer processes in host-guest-systems](#)

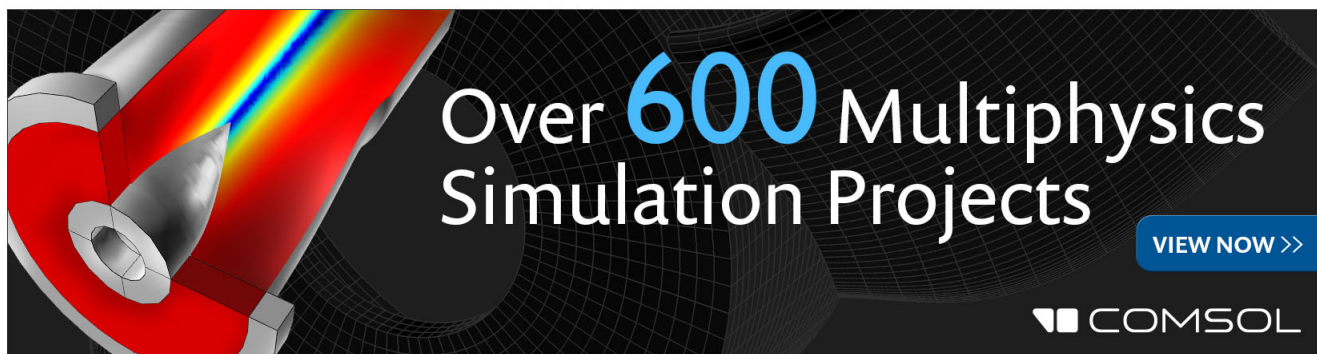
J. Appl. Phys. **111**, 033102 (2012); 10.1063/1.3679549

[Color control of multilayer stacked white polymer light-emitting diodes using a quantum dot as an interlayer](#)

Appl. Phys. Lett. **94**, 093303 (2009); 10.1063/1.3079814

[Efficient nondoped white organic light-emitting diodes based on electromers](#)

Appl. Phys. Lett. **89**, 123503 (2006); 10.1063/1.2357008

The advertisement features a dark background with a grid pattern. On the left, there is a 3D cutaway illustration of a cylindrical component with a red interior and a blue light beam passing through it. The text 'Over 600 Multiphysics Simulation Projects' is prominently displayed in the center in a large, white, sans-serif font. To the right of this text is a blue button with the text 'VIEW NOW >>'. In the bottom right corner, the COMSOL logo is visible, consisting of a small square icon followed by the word 'COMSOL' in a white, sans-serif font.

Efficient three-color white organic light-emitting diodes with a spaced multilayer emitting structure

Fei Yan,¹ Guichuan Xing,² Rui Chen,^{2,3} Hilmi Volkan Demir,^{1,2} Handong Sun,^{2,4,a)} Tze Chien Sum,^{2,a)} and Xiao Wei Sun^{1,a)}

¹LUMINOUS! Center of Excellence for Semiconductor Lighting and Displays, School of Electrical and Electronic Engineering, Nanyang Technological University, 50 Nanyang Avenue, Singapore 639798

²Division of Physics and Applied Physics, School of Physical and Mathematical Sciences, Nanyang Technological University, Singapore 637371

³Department of Electrical and Electronic Engineering, South University of Science and Technology of China, Shenzhen, Guangdong 518055, People's Republic of China

⁴Centre for Disruptive Photonic Technologies (CDPT), Nanyang Technological University, Singapore, Singapore 637371

(Received 21 October 2014; accepted 26 December 2014; published online 12 January 2015)

By employing a spaced multilayer structure in a uniformly mixed P and N co-host, we developed a three-color white organic light emitting device with a stable Commission Internationale de L'Eclairage coordinates insensitive to the applied bias voltage. This insensitivity was achieved by suppressing the exciton quenching and shifting recombination zone effectively. Besides the achieved stable color coordinates of $(0.411 \pm 0.007, 0.382 \pm 0.003)$, a high power efficiency of 30.7 lm/W and high color rendering index >80 were realized simultaneously. © 2015 AIP Publishing LLC.

[<http://dx.doi.org/10.1063/1.4905599>]

As a new technology in flat panel displays, organic light-emitting diode (OLED) displays have achieved a great success, which have been visibly demonstrated by the commercial 55" TV manufactured by LG and Samsung.^{1–10} As the next important application, OLED lighting is lags behind relatively in the commercial aspect. Although white OLED (WOLED) has not demonstrated itself as a lighting device in the commercial market, it is actually used for the state-of-the-art OLED TV-despite of the patterning difficulty in OLED displays.¹¹ Thus, it is interesting to recognize that OLED display and WOLED lighting are becoming one technology, and their development will converge. The requirements for WOLED include high power efficiency under high luminance (namely, high luminous efficiency and low driving voltage), high color rendering index (CRI), and voltage independent emission spectra.^{1–10}

To achieve white emission, there are mainly two scenarios. The first is the device with one white emissive layer doped with red (R), green (G), and blue (B) dopants. While the other one is the device containing stacked RGB emissive sub-layers. Considering both display and lighting applications, the latter one becomes the present choice.^{7,8,12–14} Normally, the mobilities of electron and hole differ by orders of magnitude or even worse for various functional layers in the OLED structure, and they are electrical field dependent.^{15,16} As a result, the recombination zone shifts with the change of driving voltage, leading to voltage dependent emissive spectra.^{8,12,13} Generally, it is difficult to obtain satisfactory performance for the parameters mentioned above for WOLED in the same device simultaneously.^{8,12,13} If the recombination zone could cover RGB emissive sub-layers uniformly at any driving voltage, the emission could be engineered to be bias-insensitive. But for

conventional structures, the recombination zone cannot extend to all the emissive sub-layers uniformly unless the thicknesses of the RGB emissive sub-layers could be decreased. However as the thickness reduces, the amount of dopant molecules is also decreased, leading to a significant drop of luminance and efficiency. In this work, we designed and realized a spaced multilayer structure (SMS) device, exhibiting high efficiency, stable spectra, and high CRI simultaneously.

All chemicals used in this work are commercially available. Patterned indium tin oxide (ITO) glass substrates ($10 \Omega/\text{sq.}$) were used in our experiments. First, the ITO substrates were cleaned with de-ionized water, isopropanol, acetone in sequence. Then they were oven-dried and treated in O_2 plasma. All functional films and aluminum electrode were fabricated by thermal evaporation in a single run at a base pressure of less than $4 \times 10^{-4} \text{ Pa}$ without breaking the vacuum. All the organics and other compounds were evaporated at a rate of about $0.1\text{--}0.2 \text{ nm s}^{-1}$, and the aluminum electrodes were evaporated at a rate of $0.8\text{--}1 \text{ nm s}^{-1}$. A shadow mask was used to define the cathode and we could obtain eight devices (with emissive area of $4 \times 4 \text{ mm}^2$) on each substrate. The luminance-current-voltage (L-I-V) characteristics and electroluminescence (EL) spectra were measured simultaneously with a Keithley 2400 source meter and a Photoresearch PR-650 spectrometer. For transient photoluminescence (PL) experiment, the laser source was Coherent Libra™ regenerative amplifier (50 fs, 1 KHz, 800 nm) seeded by a Coherent Vitesse™ oscillator (50 fs, 80 MHz). 325-nm laser pulses were generated from the Coherent OPerA-Solo optical parametric amplifier. The laser pulses (circular spot, diameter 1.5 mm) were directed to the films. The emission from the samples was collected at a backscattering angle of 150° by a pair of lenses into an Optronis Optoscope™ streak camera system which has an ultimate temporal resolution of

^{a)} Authors to whom correspondence should be addressed. Electronic addresses: hdsun@ntu.edu.sg, tzechien@ntu.edu.sg, and exwsun@ntu.edu.sg

~10 ps. All measurements were carried out at room temperature in ambient atmosphere.

Both P and N doping were applied to the charge injection layers to lower down the driving voltage and enhance the power efficiency; 4,4',4''-tris(N-3-methylphenyl-N-phenylamino)triphenylamine (m-MTDATA) doped with 2,3,5,6-tetrafluoro-7,7,8,8-tetracyanoquinodimethane (F4-TCNQ), and 3,5-Tris(1-phenyl-1H-benzimidazol-2-yl)benzene (TPBi) doped with cesium carbonate (Cs_2CO_3) were used as P-type hole injection and N-type electron injection layer, respectively. For the emissive layer (EML), a blended film of 4,4',4''-Tri-9-carbazolyltriphenylamine (TCTA) and TPBi with a 1:1 weight ratio was employed as the PN co-host for better charge balance. The phosphorescent materials of bis(1-phenyl-isoquinoline)(acetylacetonato)iridium(III) ($\text{Ir}(\text{piq})_2\text{acac}$) and bis(3,5-difluoro-2-(2-pyridyl)phenyl-(2-arboxypyridyl)iridium(III) (Flrpic) were selected as red and blue emitting dopants, respectively. In order to obtain a high CRI white emissive spectrum, the bis(2-phenylbenzothiazolato)(acetylacetonato)iridium(III) ($(\text{BT})_2\text{Iracac}$) was selected as the complementary yellow emitting dopant. The hole transport material used was N,N'-di(naphthalene-1-yl)-N,N'-iphenyl-benzidine (NPB).

The PN co-host is supposed to have a broader recombination zone compared to single host, resulting in a lower concentration of both polarons and excitons.^{17,18} Furthermore, the broader emission zone is beneficial to cover multi monochromic emission sub-layer in the WOLEDs for a voltage independent emissive spectrum. In order to investigate the influence of SMS comparing to normal emissive structure, we fabricated the blue monochrome emissive device before the WOLEDs. Four OLEDs of the PN co-host structure were fabricated and compared (Fig. 1); Device i: ITO/m-MTDATA:F4-TCNQ (5% wt., 30 nm)/NPB (15 nm)/TCTA (15 nm)/EMi/TPBi (30 nm)/TPBi: Cs_2CO_3 (10% wt., 30 nm)/Al (100 nm), where $i = 1, 2, 3,$ and 4. The structures of all EMi are indicated in Table I. The R, Y, and B represent the red TcTa:TPBi: $\text{Ir}(\text{piq})_2\text{acac}$ (1:1:x% wt.), yellow TCTA:TPBi:($\text{BT})_2\text{Iracac}$ (1:1:x% wt.), and blue TCTA:TPBi:Flrpic (1:1:x% wt.) emissive sub-layer, respectively. In the devices with the SMS, the host of TCTA:TPBi (1:1 wt) film between the emitting layers was also called spacer (S).

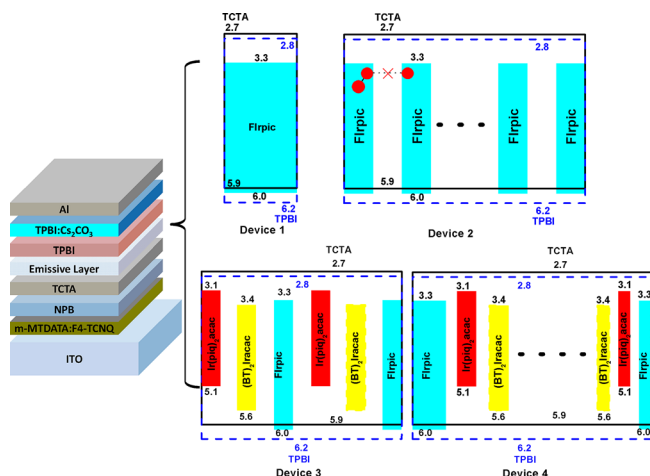


FIG. 1. The structures of devices 1, 2, 3, and 4.

TABLE I. The EM structure of all devices. The R, Y, and B represent the red TcTa:TPBi: $\text{Ir}(\text{piq})_2\text{acac}$ (1:1:x% wt.), yellow TCTA:TPBi:($\text{BT})_2\text{Iracac}$ (1:1:x% wt.), and blue TCTA:TPBi:Flrpic (1:1:x% wt.) emissive sub-layer, respectively.

Device	Emissive layer structure
EM1	B (7% wt., 20 nm)
EM2	[B (7% wt., 3.5 nm)\S (3 nm)]*5\B (7% wt., 2.5 nm)
EM3	R (7% wt., 3 nm)\S (3 nm)\Y (7% wt., 3 nm)\S (3 nm)\B (7% wt., 4 nm)\S (3 nm)\R (7% wt., 3 nm)\S (3 nm)\Y (7% wt., 3 nm)\S (3 nm)\B (7% wt., 4 nm)
EM4	B (7% wt., 5 nm)\S (2 nm)\R (5% wt., 2 nm)\S (2 nm)\Y (5% wt., 2 nm)\S (2 nm)\B (7% wt., 3 nm)\S (2 nm)\Y (5% wt., 1.5 nm)\S (2 nm)\R (5% wt., 1.5 nm)\S (2 nm)\B (7% wt., 2 nm)\S (2 nm)\Y (5% wt., 0.5 nm)\S (2 nm)\R (5% wt., 0.5 nm)\S (2 nm)\B (10% wt., 2 nm).

Device 1 is a monochrome control device with a normal guest-host structure. Device 2 is another monochrome control device with the SMS. Device 3 is the three-color white device with the SMS. Device 4 is the target three-color white device based on device 3. For all devices, the amount of all three color dopant molecules is the same.

Fig. 2 shows the plots of current density-voltage, luminous efficiency-luminance, and power efficiency-luminance of devices 1, 2, 3, and 4. For the monochrome OLED device 1, the onset driving voltage (at about 1 cd/m^2) was about 2.6 V (Fig. 2), which is close to the photon energy radiated from Flrpic exciton (478 nm). Due to the P and N doped injection layers and uniform host, there is almost no energy barrier for holes and electrons to inject and transport. Additionally, because of a better charge balance of the P and N co-host, the device shows a maximum luminous efficiency of about 37.3 cd/A at 150 cd/m^2 and a maximum power efficiency of about 42.1 lm/W at 3.5 cd/m^2 . Comparing to device 1, the maximum luminous efficiency of device 2 with the SMS is 35.9 cd/A at 143 cd/m^2 , slightly lower compared to device 1, which is probably caused by the backward energy transfer from Flrpic exciton to TPBi (triplet state of 2.6 eV) molecule in the spacer between two emissive sub-layers.⁷ Additionally, the driving voltage of device 2 with the SMS is

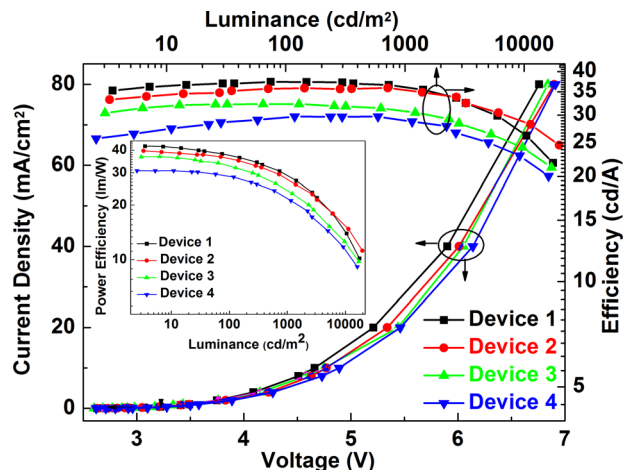


FIG. 2. The current density-voltage and luminous efficiency-luminance curves of devices 1, 2, 3, and 4. The power efficiency plots versus luminance of devices 1, 2, 3, and 4 are shown in inset.

slightly higher comparing to device 1, which is related to more interfaces of the SMS. The maximum power efficiency of device 2 was 39.6 lm/W at 3.3 cd/m². However, it is noted that the luminous efficiency drop for device 2 (dropped by 21% from 35.9 cd/A at 143 cd/m² to 28.2 cd/A at 11290 cd/m²) at high luminance was improved significantly compared to device 1 (dropped by 36% from 37.3 cd/A at 150 cd/m² to 26.1 cd/A at 10470 cd/m²). Though the amount of monochromic dopant molecules is the same for devices 1 and 2, and the concentration of dopant for each emissive sub-layer in device 2 is also the same to device 1, due to the spaced recombination zone structure, the distance between two Ir-complex dopants divided by the spacer exceeds the effective radius of exciton-exciton interactions (Fig. 1). Thus, the triplet-triplet exciton annihilation process caused by exciton-exciton interaction, especially under higher driving current density, was suppressed effectively, leading to a slower luminous efficiency roll-off.^{17–19} In order to compare the luminous efficiency droop between devices 1 and 2, following Baldo *et al.*,²⁰ we defined a critical current density (J_0) as the luminous efficiency drop to 70% of the maximum value. As indicated in Fig. 2, for device 1, J_0 is about 40 mA/cm² when the luminous efficiency is 26.1 cd/A (the corresponding maximum luminous efficiency is 37.3 cd/A at 0.2 mA/cm²). While for device 2 with SMS, J_0 is about 80 mA/cm² when the luminous efficiency is 24.5 cd/A, compared to the maximum luminous efficiency of 35.8 cd/A at 0.4 mA/cm².

Based on the above works, the three-color white device 3 with the SMS was fabricated, and the maximum luminous efficiency is about 32.2 cd/A at 64.5 cd/m² (dropped by 24.8% to 24.2 cd/A at 9690 cd/m²) (Fig. 2), which is comparatively smaller than those of devices 1 and 2. The maximum power efficiency was about 36.8 lm/W at 3.1 cd/m² and it decreased to 12.5 lm/W at 9690 cd/m², which accounts for about 66% reduction. As Fig. 3(a) shows, the blue component dominates initially, and as the driving voltage increases, the spectra shift significantly. As shown in the inset of Fig. 3(a), the Commission Internationale de L'Éclairage (CIE) 1931 coordinates change significantly from (0.209, 0.403) at 13 cd/m² to (0.428, 0.427) at 9690 cd/m². A similar phenomenon was observed by changing the sequence of monochromic emissive sub-layers. Though the P and N co-host architecture facilitates a broader recombination zone and better charge balance compared to the single host device, due to a higher hole mobility of TCTA (in comparison to the electron mobility of TPBi) and a faster increasing electron mobility of TPBi (comparing to the hole mobility of TCTA) with the increase of driving voltage, the recombination zone becomes highly voltage dependent.^{18,21} At a low driving voltage, the recombination zone mainly distributes at the EML/electron transport layer (ETL) interface with an energy barrier for hole transport, thus the emission of FIrpic is dominated. As driving voltage increases, the recombination zone extends and shifts towards the EML/hole transport layer (HTL) interface, leading to a significant emissive spectrum shift. If the recombination zone can always cover three different monochromic emissive sub-layers at any driving voltage, the emissive spectral shift can be suppressed effectively. Thus the spacer and emissive sub-layer must be thin enough.

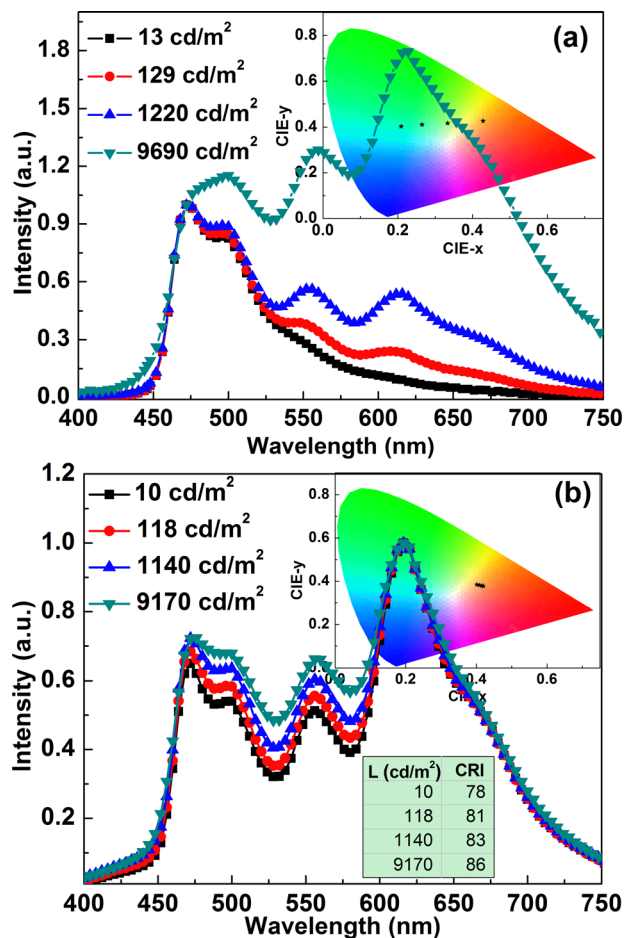


FIG. 3. (a) The emissive spectra of device 3 at different luminance, and the inset indicates the corresponding CIE coordinates. (b) The emissive spectra of device 4 at different luminance, and the inset and table show the corresponding CIE coordinates and CRI, respectively.

Additionally, the energy transfer processes from higher energy dopant excitons to the lower ones probably play an important role in the spectral shift. Though the shorter Förster energy transfer radii (less than 2 nm) for Ir-complex and the higher triplet state energy (2.8 eV) of TCTA can suppress the spectral shift by partially blocking the Förster and Dexter energy transfer processes between two adjacent emitting layers, the energy transfer processes via TPBi triplet state may still exist.⁷ In order to investigate the potential energy transfer between the B, Y, and R emitters, the time-resolved photoluminescence (TRPL) of individual emitter films were collected. The decay traces of the emission peaks (± 5 nm) were presented in Figure 4. The PL lifetimes are fitted as 1.33 μ s, 1.21 μ s, and 0.87 μ s for the single layers containing FIrpic, (BT)₂Iracac, and Ir(piq)₂acac, respectively. It can be seen from Figure 4 clearly that the decay trace for the relative high photon energy emitter in the bi-emitter film is almost overlapped with the corresponding single layer decay trace. The changes in exciton lifetime should be quite significant, especially for the energy donor, should there be any effective non-radiative energy transfer between two different Ir-complexes. In view of the large distance between two Ir-complexes, this suggests that the energy transfer between the different monochromic emitters in the bi-layer films is inefficient. The slightly increased lifetime for the relative low

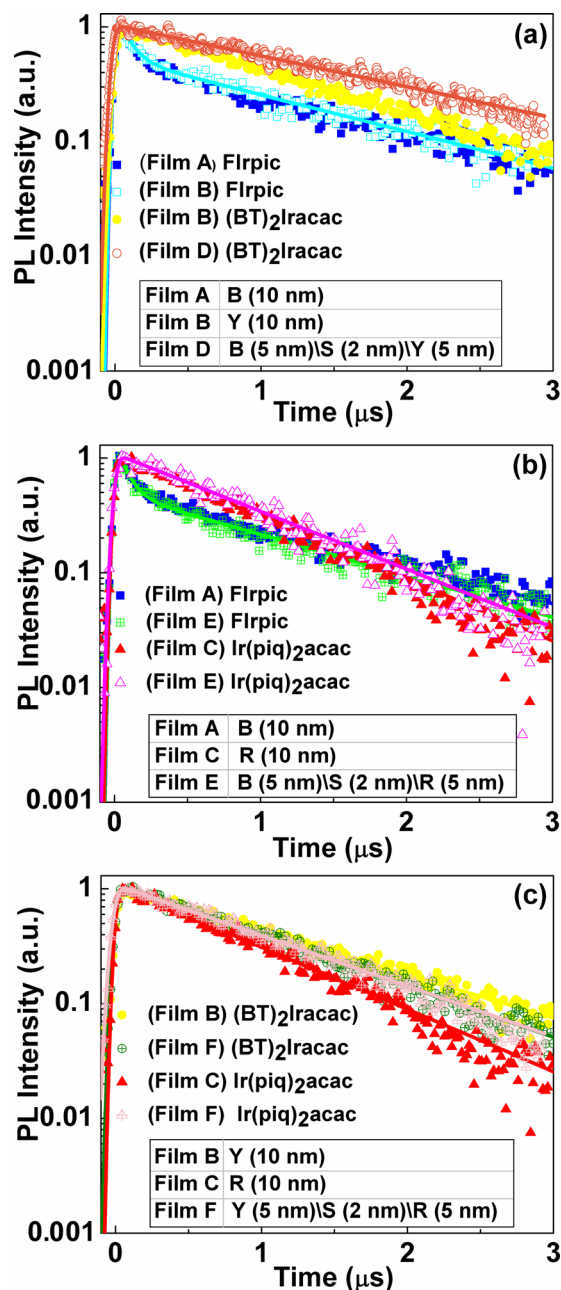


FIG. 4. The transient photoluminescence plots of (a) Firpic in film A and D (monitored at 478 nm), and (BT)₂Iracac in films B and D (monitored at 560 nm), (b) Firpic in films A and E (monitored at 478 nm), and Ir(piq)₂acac in films C and E (monitored at 620 nm), (c) (BT)₂Iracac in films B and F (monitored at 560 nm), and Ir(piq)₂acac in films C and F (monitored at 620 nm). The solid lines are correspondingly fitting curves. The R, Y, and B represent the TeTa:TPBi:Ir(piq)₂acac (1:1:7% wt.), TCTA:TPBi:(BT)₂Iracac (1:1:7% wt.), and TCTA:TPBi:Firpic (1:1:7% wt.) film, respectively.

photon energy emitter in the bi-emitter film should be caused by the relative high energy photon re-absorbed by this emitter.²²

To weaken the spectral shift caused by the recombination zone shift and re-absorption of lower emitters, the thickness of emissive sub-layers and spacer were reduced for device 4 compared to device 3. Furthermore, in order to weaken the influence of non-radiative energy transfer process, the amounts of all monochromatic dopant in the emissive sub-layers were adjusted, and the optimized three-color white device 4 was designed and fabricated. Because there is

a relatively thicker and larger energy barriers for electron and hole at EML\HTL and EML\ETL interfaces, respectively, the charge and exciton densities are correspondingly larger. Thus, we allocated the two blue monochromatic layers at these two interfaces to ensure the relative intensity of Firpic compared to the other two components. Similarly, in order to weaken the likely influence of non-radiative energy transfer, the sequence of the monochromatic layers were also adjusted to ensure the spectral stability. From the spectral shift indicated in Fig. 3(a) and emission layer structure of device 3 (Fig. 1), the recombination zone width was extended from less than 9 nm to more than 16 nm. A spacer thickness of 2 nm was selected for in device 4, which is to balance the spectral shift caused by recombination zone shift and energy transfer between different emissive excitons. To ensure a stable emission of blue color as the driving voltage varies, the Firpic concentration of the emissive sub-layer close to EML\ETL interface was increased to 10% wt., and the amount of Firpic in the whole emissive layer is more than those of (BT)₂Iracac and Ir(piq)₂acac. As Fig. 2 shows, device 4 exhibits a maximum luminous efficiency of about 29.7 cd/A at 118 cd/m², which reduces to 22.9 cd/A at 9170 cd/m². The corresponding drop is about 22%. The power efficiency of the device is 30.7 lm/W at 5.7 cd/m² and 11.7 lm/W at 9170 cd/m², which accounts for 60% drop. As shown in Fig. 3(b), the CIE 1931 coordinates of device 4 fall in the warm white range. As the driving voltage varies, coordinates (0.411 ± 0.007, 0.382 ± 0.003) have a little change as the luminance increases from about 10 cd/m² to about 10 000 cd/m². Additionally, the CRIs at various luminance are also excellent as indicated in the inset table in Fig. 3(b); at about 10 000 cd/m², the CRI is 86.

In conclusion, employing P and N doped charge injection layer, P and N co-host, and SMS emissive layer, a three-color WOLED was developed, which exhibited a good overall performance, including high power efficiency, slower efficiency roll off at high luminance, stable emissive spectra, and high CRI.

This work was financially supported by National Research Foundation of Singapore (Grant Nos. NRF-CRP11-2012-01 and NRF-CRP6-2010-2).

¹S. Kalluri, R. R. Jerry, and C. Charles, in Conference on Head- and Helmet-Mounted Displays XVII/Conference on Display Technologies and Applications for Defense, Security, and Avionics VI, Baltimore, MD, 25–26 April 2012.

²Z. Ma, P. Sonar, and Z. Chen, *Curr. Org. Chem.* **14**, 2034–2069 (2010).

³A. Laaperi, *J. Soc. Inf. Disp.* **16**, 1125–1130 (2008).

⁴O. N. Ermakov, M. G. Kaplunov, O. N. Efimov, and S. A. Stakharny, *Proc. SPIE* **6636**, A6360 (2007).

⁵Y. L. Lei, Y. Jin, D. Y. Zhou, W. Gu, X. B. Shi, L. S. Liao, and S. T. Lee, *Adv. Mater.* **24**, 5345 (2012).

⁶H. Sasabe, J. Takamatsu, T. Motoyama, S. Watanabe, G. Wagenblast, N. Langer, O. Molt, E. Fuchs, C. Lennartz, and J. Kido, *Adv. Mater.* **22**, 5003–5007 (2010).

⁷S. Reineke, F. Lindner, G. Schwartz, N. Seidler, K. Walzer, B. Lüsslem, and K. Leo, *Nature* **459**, 234–238 (2009).

⁸C. Murawski, K. Leo, and M. C. Gather, *Adv. Mater.* **25**, 6801–6827 (2013).

⁹B. W. D'Andrade and S. R. Forrest, *Adv. Mater.* **16**, 1585–1595 (2004).

¹⁰B. W. D'Andrade, J. Brooks, V. Adamovich, M. E. Thompson, and S. R. Forrest, *Adv. Mater.* **14**, 1032–1036 (2002).

- ¹¹C. W. Han, K. M. Kim, S. J. Bae, H. S. Choi, J. M. Lee, T. S. Kim, Y. H. Tak, S. Y. Cha, and B. C. Ahn, *Dig. Tech. Pap. - Soc. Inf. Disp. Int. Symp.* **43**, 279–281 (2012).
- ¹²M. C. Gather, R. Alle, H. Becker, and K. Meerholz, *Adv. Mater.* **19**, 4460 (2007).
- ¹³A. Köhnen, K. Meerholz, M. Hagemann, M. Brinkmann, and S. Sinzinger, *Appl. Phys. Lett.* **92**, 33305 (2008).
- ¹⁴B. Zhao, Z. Su, W. Li, B. Chu, F. Jin, X. Yan, T. Zhang, F. Zhang, D. Fan, Y. Gao, J. Wang, H. Pi, and J. Zhu, *Nanoscale Res. Lett.* **8**, 529 (2013).
- ¹⁵A. Köhler, *Nat. Mater.* **11**, 836–837 (2012).
- ¹⁶T. I. Fishchuk, A. Kadashchuk, M. Ullah, H. Sitter, A. Pivrikas, J. Genoe, and H. Bässler, *Phys. Rev. B* **86**, 045207 (2012).
- ¹⁷S. Lee, K. Kim, D. Limbach, Y. Park, and J. Kim, *Adv. Funct. Mater.* **23**, 4105–4110 (2013).
- ¹⁸S. Kim, J. Jang, K. Yook, and J. Lee, *Appl. Phys. Lett.* **92**, 023513 (2008).
- ¹⁹M. Gather, A. Köhnen, and K. Meerholz, *Adv. Mater.* **23**, 233–248 (2011).
- ²⁰M. A. Baldo, C. Adachi, and S. R. Forrest, *Phys. Rev. B* **62**, 10967 (2000).
- ²¹L. Xia, Z. Chen, B. Qu, J. Luo, S. Kong, Q. Gong, and J. Kido, *Adv. Mater.* **23**, 926–952 (2011).
- ²²M. I. Sluch, A. S. Averjushkin, O. I. Tolstikhin, and A. G. Vitukhnovsky, *Phys. Scr.* **50**, 585 (1994).